Title

Sensory neurons expressing calcitonin gene-related peptide α regulate adaptive thermogenesis and diet-induced obesity

Authors

Makwana, Kuldeep
Chodavarapu, Harshita
Morones, Nancy
et al.

Peer reviewed

Sensory neurons expressing calcitonin gene-related peptide α regulate adaptive thermogenesis and diet-induced obesity

Kuldeep Makwana [1,4], Harshita Chodavarapu [1,4], Nancy Morones [1], Jingyi Chi [2], William Barr [3], Edward Novinbakht [1], Yidan Wang [1], Peter Tuan Nguyen [1], Predrag Jovanovic [1], Paul Cohen [2], Celine E. Riera [1,3,*]

ABSTRACT

Objectives: Heat-sensory neurons from the dorsal root ganglia (DRG) play a pivotal role in detecting the cutaneous temperature and transmission of external signals to the brain, ensuring the maintenance of thermoregulation. However, whether these thermoreceptor neurons contribute to adaptive thermogenesis remains elusive. It is also unknown whether these neurons play a role in obesity and energy metabolism.

Methods: We used genetic ablation of heat-sensing neurons expressing calcitonin gene-related peptide α (CGRPα) to assess whole-body energy expenditure, weight gain, glucose tolerance, and insulin sensitivity in normal chow and high-fat diet-fed mice. *Exvivo* lipolysis and transcriptional characterization were combined with adipose tissue-clearing methods to visualize and probe the role of sensory nerves in adipose tissue. Adaptive thermogenesis was explored using infrared imaging of intrascapular brown adipose tissue (iBAT), tail, and core temperature upon various stimuli including diet, external temperature, and the cooling agent icilin.

Results: In this report, we show that genetic ablation of heat-sensing CGRPα neurons promotes resistance to weight gain upon high-fat diet (HFD) feeding and increases energy expenditure in mice. Mechanistically, we found that loss of CGRPα-expressing sensory neurons was associated with reduced lipid deposition in adipose tissue, enhanced expression of fatty acid oxidation genes, higher *exvivo* lipolysis in primary white adipocytes, and increased mitochondrial respiration from iBAT. Remarkably, mice lacking CGRPα sensory neurons manifested increased tail cutaneous vasoconstriction at room temperature. This exacerbated cold perception was not associated with reduced core temperature, suggesting that heat production and heat conservation mechanisms were engaged. Specific denervation of CGRPα neurons in intrascapular BAT did not contribute to the increased metabolic rate observed upon global sensory denervation.

Conclusions: Taken together, these findings highlight an important role of cutaneous thermoreceptors in regulating energy metabolism by triggering counter-regulatory responses involving energy dissipation processes including lipid fuel utilization and cutaneous vasodilation.

1. INTRODUCTION

Organismal survival is highly dependent on the tight regulation of body core temperature. Dedicated central neural circuits respond to deviations in endogenous and exogenous temperatures through counter-regulatory measures with an autonomic nature [1]. Warm environments elicit involuntary autonomic measures to reduce thermogenesis and increase cutaneous vasodilation and sweating to release heat. Conversely, cold perception triggers gradual autonomic responses starting with vasoconstriction of cutaneous vessels to reduce heat loss through the skin. If mild cold exposure persists, non-shivering (adaptive) thermogenesis results in increased energy expenditure due to the activation of thermogenic mechanisms in adipose tissue to produce heat [1,2].

A fundamental component of engaging central and sympathetic thermoregulatory measures is the detection and integration of signals provided by cutaneous thermoreceptors, which are primary sensory nerve endings located in the skin [3,4]. These nerves contain transient receptor potential (TRP) channels with specific temperature conductance allowing them to sense cool and warm temperatures. Warm sensing is mediated by TRPV1 [5,6], whereas cooling is perceived by TRPM8 [7,8]. These spinal sensory nociceptor fibers arise from the dorsal root ganglion (DRG) and are both peptidergic and non-peptidergic in nature. CGRP and substance P constitute the most widely recognized markers in the peptidergic category [9]. Primary sensory neurons expressing CGRPα overlap with the sensory receptor TRPV1 but are segregated from TRPM8-expressing neurons [10]. As

[1]Center for Neural Science and Medicine, Department of Biomedical Sciences, Board of Governors of the Regenerative Medicine Institute, Department of Neurology, Cedars-Sinai Medical Center, 127 South San Vicente Boulevard, Los Angeles, CA, USA [2]Laboratory of Molecular Metabolism, The Rockefeller University, New York, NY, USA [3]David Geffen School of Medicine, University of California, Los Angeles, CA, USA

[4] Kuldeep Makwana and Harshita Chodavarapu contributed equally to this work.

*Corresponding author. 127 S. San Vicente Blvd., Advanced Health Sciences Pavilion, Suite A8305, Los Angeles, CA, 90048, USA. E-mail: celine.riera@cshs.org (C.E. Riera).

expected, CGRPα neurons respond to the selective TRPV1 agonist capsaicin, but are insensitive to the TRPM8 agonist icilin [10].

Much evidence links TRPV1 channel modulation to changes in energy metabolism and body weight homeostasis. Capsinoids have proven efficient at reducing weight gain, and TRPV1 knock-out mice are protected from diet-induced obesity (DIO) [11—16]. Age-dependent metabolic decline is prevented by TRPV1 mutation and inhibition of CGRP receptors with infusion of a peptide antagonist [17]. However, TRPV1 is also present in the arcuate nucleus of the hypothalamus where it blocks feeding upon exercise-generated heat [18]. Therefore, the specific role of spinal TRPV1 neurons in energy metabolism remains difficult to disentangle from the central effects of the receptor. Changes in adaptive thermogenesis occur during cold challenge but also in response to diet. Remarkably, a calorie-dense diet triggers an increase in energy expenditure as a counter-regulatory measure from the central nervous system (CNS) to dissipate these additional calories [19,20]. Because of the role of TRPV1 receptors in temperature detection and energy metabolism, we examined the potential recruitment of peripheral neurons in adaptive thermogenesis in response to DIO. To clarify the role of heat-sensing DRGs in energy metabolism, we used a genetic strategy to ablate CGRPα-containing sensory neurons in the periphery and investigated animals' alterations in adaptive thermogenesis. In this report, we provide direct evidence that loss of CGRPα-positive sensory neurons potentiates diet-dependent thermogenesis through increased sensitivity to cold perception.

2. MATERIALS AND METHODS

2.1. Experimental design

All of the procedures were approved by the Animal Care and Use Committee of Cedars Sinai Medical Center. Ablation of mature CGRPα sensory neurons in adult mice was achieved by expressing the inducible diphtheria toxin receptor (DTR) specifically in advillin (Avil)-positive sensory neurons and conditional ablation by diphtheria toxin (DT) administration as previously described [21]. Advillin-Cre mice were a donation from Fan Wang (Duke University) and $Calca^{-<lox-GFP-lox-hDTR>}$ mice were donated by Marc Zylka (UNC Chapel Hill). To perform sensory ablation, DT (40 ng/g) was intraperitoneally administered in 5-week-old mice twice within a 48-hour window. Three cohorts of male mice were respectively placed on DIO for 6, 8, and 17 weeks and compared with NC-fed animals. To specifically ablate sensory fibers in intrascapular brown adipose tissue (iBAT), an incision was made above the iBAT to expose the fat pads, and 6 microinjections of 0.5 μL of DT (5 ng/μL) were given to each pad followed by sutures to close the wound. The mice were fed normal chow (PicoLab Rodent 20 5053, LabDiet) until 6 weeks of age and switched to either HFD chow (BioServ, 60% fat calories) or normal chow (NC). Chemical cooling was achieved by intraperitoneal administration of icilin (0.6 mg/kg; Sigma—Aldrich) dissolved in sterile saline.

2.2. Indirect calorimetry, physical activity, and food intake

Indirect calorimetric studies were conducted in an automated home cage eight-chamber phenotyping system (Phenomaster, TSE). Body composition was assessed by EchoMRI. The mice were acclimatized in the chambers for at least 24 h. Food and water were provided ad libitum in the appropriate devices and measured by built-in automated instruments. Locomotor activity and parameters of indirect calorimetry were measured for at least the following 48 h. Intraperitoneal injections of CL316243 (1 mg/kg, Sigma—Aldrich) dissolved in sterile saline were given followed by measurement of oxygen consumption, activity, food intake, and EchoMRI.

2.3. Metabolic studies

To perform the GTT, the mice were fasted for 16 h and their tails were bled for the initial blood glucose concentration measured using a One Touch Ultra glucometer (LifeScan) or Bayer Contour glucometer (Bayer). Glucose (2 g/kg weight) was intraperitoneally administered, and blood glucose was measured at indicated times after injection. For the ITT, 5-hour fasted mice were injected with 1 u/kg of human insulin (Humulin; Eli Lily) and glucose was measured as in the GTT. For cold tolerance assays, the mice were acclimated at 28 °C for 48 h and subjected to 4 °C for 4—6 h. rectal temperature was recorded every hour.

2.4. Hot plate test

The mice were subjected to 3 trials separated by 30-minute intervals at 52 °C on a Hot Plate Analgesia Meter (IITC). Signs including paw shaking and licking were used as discomfort toward temperature perception, and the latency to achieve these behaviors was recorded.

2.5. Quantitative PCR analysis

RNA was isolated using TRIzol/chloroform extraction and RNEasy Qiagen columns. Gene expression was assessed by qPCR Applied Biosystems Power SYBR Green RNA-to-CT 1-Step Kit. The 18s gene was used as a control, and 25 ng of total RNA was used for each reaction.

2.6. RNA sequencing

RNA was isolated from adipose tissues as previously mentioned. RNA samples from 3 biological replicates each for the control and treated groups were processed at the genomics core at Cedars Sinai Medical Center. The poly A tail selection method for enrichment of mRNAs and a non-stranded single-end library was prepared for sequencing. Novaseq 6000 was used for sequencing. Quality analysis of Fastq files was done using FastQC (https://www.bioinformatics.babraham.ac.uk/projects/fastqc). Reads were aligned to the mouse reference genome (GRCm38.p5 Release M21) using STAR [22]. Count tables were generated using HTSeq (options: stranded = no and mode = union). Differential gene expression analysis was performed using DESeq2 [23]. Transcripts with p values for false discovery less than 0.049, mean base >100 across samples, and log2 value > 0.7 or < −0.7 were shortlisted for further analysis. A KEGG pathway analysis on shortlisted transcripts was done using Database for Annotation, Visualization, and Integrated Discovery (DAVID) v6.8 bioinformatics resources [24].

2.7. Protein analysis

Adipose tissue was homogenized in TNET buffer (50 mM of Tris—HCl, 5 mM of EDTA, and 150 mM of NaCl) supplemented with complete protease inhibitor tablets (Roche) and PhosSTOP (Roche). Protein concentrations were determined using BCA (Pierce). A total of 20—50 μg of samples were loaded on SDS/Page gels (Invitrogen) then transferred to nitrocellulose membranes. Ponceau-S staining was used to confirm equal loading. Immunoblotting was done in 5% BSA containing TBS-T with antibodies against β-tubulin (Cell Signaling Technology) and TH (EMD Millipore) at a concentration of 1:1000.

2.8. Immunofluorescence and histological studies

The animals were perfused with 4% paraformaldehyde prior to sacrifice. The tissues were cryoprotected in 30% sucrose in PBS overnight, frozen in OCT (Tissue-Tek), and sectioned on a cryostat. Then, 12-μm-thick sections were immunoblotted with primary antibodies in PBS containing 2% donkey serum and 0.4% Triton x100. Antibodies

used were anti-CGRPα (Enzo) at 1:100 and anti-GFP (Thermo Fisher Scientific) at 1:200, and secondary antibodies (Alexa) were diluted at 1:600. For histological analysis, the tissues were immersed in formalin overnight, dried in 70% ethanol, and embedded in paraffin. Then 8-μm-thick sections were stained with hematoxylin and eosin. The sections were imaged using a Keyence microscope BZ-X700. For adipose tissue immunostaining, the tissues were first delipidated and permeabilized as previously described [25]. BAT frozen tissue sections were then cut into 50-μm sections and processed for immunohisto-chemistry. Gonadal and inguinal WAT samples were processed for whole fat pad staining and light sheet microscopy [25].

2.9. Temperature recordings

Animal colonies were maintained at 22 °C. Core body temperature recordings were measured using a rectal probe. Intrascapular BAT and tail temperatures were obtained with Flir E60bx or E75 thermal cameras and analyzed with QuickReport software to extract tem-perature recordings of the iBAT area and the base of the tail. For recordings at 28 °C, the animals were first acclimatized at 28 °C for two days and their temperatures were recorded on the third day.

2.10. Statistical methods

Statistical analyses were performed using GraphPad Prism version 9. All of the statistical analyses were two-sided. When comparing the two groups, two-tailed unpaired Student's t-test was used to determine the significance of the experimental results. For experiments with a two-factorial design, two-way ANOVA was performed to establish that not all of the groups were equal. The Holm-Sidak post hoc analysis was then used for specific between-group comparisons after statistical significance was established by ANOVA. In each case, significance was set at $p = 0.05$.

3. RESULTS

3.1. Loss of CGRP nociceptors blocked diet-induced obesity in mice

We used a selective strategy to ablate CGRPα-containing sensory neurons by crossing $Calca^{-<lox-GFP-lox-hDTR>}$ knock-in mice [10,21] to advillin-Cre mice [26]. Combined, advillin and Calca (encoding for CGRPα) promoters restrict the transgene expression to CGRPα-expressing sensory neurons arising from the DRG [10,21]. $Calca^{-<lox-GFP-lox-hDTR>}$ knock-in is characterized by a floxed (loxP flanked) axonal GFP tracer knocked into the Calca locus to block the expression of downstream DTR, which is expressed upon Cre-dependent recombination. This strategy allows the ablation of nerve fibers by injecting DT in adult animals, thus controlling the temporal inactivation of selected nerves and avoiding compensatory effects that can occur during development (Figure 1A). DT injection specifically ablates CGRPα cell bodies in DRG ganglia and associated afferents in the dorsal spinal cord, specifically impairing animals' ability to respond to TRPV1-dependent sensory stimuli (capsaicin and heat) [21]. To confirm loss of CGRPα neurons, we performed immunohistochemistry (IHC) of DRGs to quantify neuronal numbers in DT-treated $Avil^{-/-}$; $Calca^{-<lox-GFP-lox-hDTR>+/-}$ (WT) and $Avil^{+/-}$; $Calca^{-<lox-GFP-lox-hDTR>+/-}$ (CGRPα−) littermates. DT administration led to almost complete depletion of DRG-CGRPα neurons as measured by GFP fluorescence (Supp. Fig. 1a ,b). The CGRPα− mice showed reduced paw withdrawal latency compared to the control WT animals 3 and 6 days following DT injection during a hot plate test (Supp. Fig. 1c). To
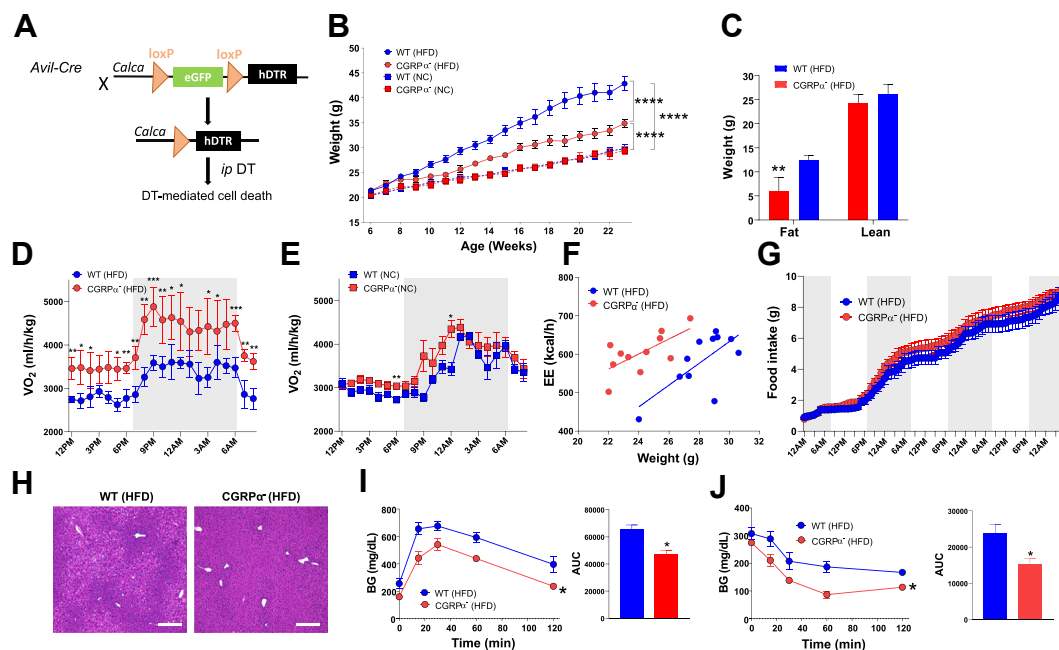

Figure 1: DT-injected CGRPα-DTR were resistant to diet-induced obesity. (A) Strategy to ablate CGRPα sensory neurons adapted from Mc Coy et al. Advillin-Cre was used to removed floxed GFP and drive human DTR in CGRPα sensory neurons. (B) Weight gain of CGRPα− and littermate controls (WT) on a normal chow diet (NC) and high-fat diet (HFD). (C) Fat and lean mass of the CGRPα− and control littermates after 12 weeks of HFD feeding. (D) VO$_2$ measured in 12-week-old HFD-fed mice. (E) Oxygen consumption in 12-week-old NC-fed mice. (F) ANCOVA analysis of energy expenditure with body weight as a covariate in 12-week-old HFD-fed mice, p < 0.005. (G) Cumulative food intake of 12-week-old HFD-fed mice measured over the course of 3 days. (H) Hematoxylin and eosin (H&E) sections of liver biopsies from the HFD-fed CGRPα− and WT mice, scale 300 μm. (I) Blood glucose (BG) levels during glucose tolerance testing and area under the curve analysis of 16-week-old HFD-fed mice. (J) Insulin tolerance testing and area under the curve analysis of 17-week-old HFD-fed mice. N = 9–11, ****p < 0.0001, ***p < 0.0001, **p < 0.001, and *p < 0.05. All the values denote means ± SEM.

verify the peripheral vs central action of DT, we analyzed the presence of CGRPα neurons in the brain and did not observe any loss in the parabrachial nucleus in the CGRPα⁻ mice (Supp. Fig. 1d), which contained a subset of CGRPα-expressing neurons [27,28]. Therefore, this model allowed for the specific depletion of peripheral CGRPα sensory neurons.

Based on previous studies implicating TRPV1 and CGRPα in weight gain and energy metabolism [14,17], we asked whether CGRPα⁻ mice developed metabolic changes on normal chow (NC) and high-fat diet (HFD). We injected DT in all of the animals and did not observe adverse effects in the wild-type C57BL/6 background, as previously reported [29]. The CGRPα⁻ mice on NC were the same weight as their wild-type (WT) littermates (Figure 1B). However, when fed a HFD, the CGRPα⁻ mice remained significantly leaner than the controls (Figure 1B) with the weight difference attributed to reduced fat mass (Figure 1C). Increased oxygen consumption (VO_2) measured by indirect calorimetry was observed in the HFD-fed animals lacking CGRPα neurons and a trend toward higher VO_2 was seen in the NC-fed CGRPα⁻ mice compared to the controls (Figure 1D,E). Analysis of covariance (ANCOVA) of energy expenditure (EE) with body mass as a covariate demonstrated increased energy metabolism in the HFD-fed CGRPα⁻ mice compared to their HFD littermates (Figure 1F). No differences in activity or food intake were observed between the genotypes on the HFD (Figure 1G) or NC (Supp. Fig. 1e). We also observed that after 17 weeks of DIO, hepatic steatosis remained minimal upon loss of CGRPα neurons (Figure 1H). The CGRPα⁻ mice had improved glucose tolerance and insulin sensitivity after 12 and 13 weeks of DIO (Figure 1I,J). We also asked if these effects were sex-specific and monitored weight gain in the female CGRPα⁻ and WT littermate animals on the HFD. As in the males, the females were also resistant to DIO despite a delayed weight gain response over time (Supp. Fig. 1g and h). The female mice also showed improved glucose tolerance upon DIO (Supp. Fig. 1i). Because of the general resistance of the female mice to obesity, we then focused on the male mice for the remainder of our study.

The ameliorated glucose homeostasis in the HFD-fed CGRPα⁻ may be due to the direct consequence of sensory afferent neuron depletion or occur as a side effect of the lower fat mass of these animals. To further investigate whether loss of CGRP neurons led to increased glucose utilization, we measured glucose tolerance in weight-matched animals on the NC and HFD. Glucose utilization was similar in the weight-matched CGRPα⁻ and WT littermates receiving the HFD for 6 weeks (Supp. Fig. j). Similarly, no difference in glucose tolerance was observed in the 20-week-old NC-fed CGRPα⁻ and WT littermates harboring similar weights (Supp. Fig. 1k).

3.2. Increased energy expenditure upon loss of CGRPα neurons partially depended on adrenergic signaling responsiveness

Sympathetic nervous system (SNS) activation is a well-established driver of thermogenesis, with SNS catecholamines released in adipose tissue promoting β-adrenergic receptor (AR) stimulation and lipolysis of stored triglycerides in both white and brown adipocytes [30]. β3-AR is the predominant adipose tissue adrenoreceptor mediating thermogenesis in BAT and lipolysis in WAT [31,32]. Released free fatty acids (FFAs) are used by BAT to drive cold- and diet-stimulated thermogenesis, generating chemical heat through uncoupling mitochondrial oxidative phosphorylation from ATP production or other mitochondrial energy−generation pathways [33,34].

Because the HFD led to elevated energy expenditure in the HFD-fed CGRPα⁻ mice (Figure 1E), we hypothesized that loss of CGRPα neurons led to enhanced β-AR activation in adipose tissue. We therefore investigated whether increased β3-AR stimulation in adipose tissue

was observed in the CGRPα⁻ mice on the NC and HFD. Acute stimulation of β3-AR through CL316,243 (CL) leads to an immediate increase in energy expenditure mediated by lipolysis and FFA oxidative metabolism [35−38]. As expected, CL injection dramatically augmented VO_2 in the weight-matched NC-fed CGRPα⁻ and WT animals (Figure 2A-C). In the first 3 h immediately following CL, a sharper elevation in VO_2 was observed in the NC-fed CGRPα⁻ mice (Figure 2B). After this initial response, the dark cycle VO_2 peak increased similarly in both the WT and CGRPα⁻ compared to vehicle treatment (Figure 2C). The increased oxidative metabolism following CL treatment was associated with an immediate decline in the respiratory exchange ratio (RER) in all of the genotypes as a consequence of substantial lipolytic activity in adipose tissue (Figure 2D). Remarkably, the RER of the CGRPα⁻ mice was higher during the dark cycles before and after CL injection (Figure 2D), indicating overall higher carbohydrate oxidation in the absence of CGRPα neurons. Food intake and ambulatory activity remained similar among the genotypes (Supp. Fig. 2a ,b).

We then examined the effects of CL on the animals after 2 weeks of the HFD before the weight difference between the HFD-CGRPα⁻ and littermate controls reached statistical significance. Most likely due to diet-induced thermogenesis, VO_2 was higher in both genotypes compared to NC (Figure 2A,E). In particular, the CGRPα⁻ animals manifested a higher degree of thermogenic response than the WT animals before CL treatment in light and dark cycles (Figure 2E), consistent with their increased energy expenditure and reduced adiposity (Figure 1C,E). Acute CL treatment further raised the VO_2 levels in both groups, with reduced amplitude in the CGRPα⁻ animals showing a higher resting metabolic rate but led to an immediate VO_2 response that was more pronounced in the CGRPα⁻ animals (Figure 2E,F). During the following dark cycle, peak VO_2 was characterized by a major elevation in the HFD-WT mice compared to pre-CL treatment (Figure 2G). In the HFD-CGRPα⁻ animals, this rise was less pronounced and reached a similar maximum than in the HFD-WT mice (Figure 2G). Consistent with increased FFA utilization during the light cycle, the HFD-CGRPα⁻ animals showed reduced RER compared to the WT pre-CL treatment (Figure 2H). CL injection led to sustained lower RER in the WT mice throughout the dark cycle, presumably because of the combined HFD and CL-dependent FFA metabolism (Figure 2H). As in the NC-fed mice, the HFD-CGRPα⁻ animals were able to switch faster to carbohydrate metabolism during the dark cycle following CL (Figure 2H). There was no significant difference in food intake or physical activity between the two genotypes, and the observed reduction in ambulatory activity upon CL was slightly more pronounced in the HFD-CGRPα⁻ mice (Supp. Fig. 2c ,d). Taken together, these observations suggest higher energy utilization in the absence of CGRPα neurons and a minor elevation of thermogenic β3-AR response. These results bring up the possibility that the CGRPα⁻ mice manifested improved adipose lipolysis and/or improved BAT thermogenesis.

3.3. Prolonged diet-induced obesity induced the expression of thermogenic and fatty acid metabolism genes in BAT in the absence of CGRPα neurons

To elucidate whether loss of CGRPα neurons leads to enhanced BAT thermogenesis, we collected biopsies of intrascapular BAT (iBAT) for histological and functional assays. While the control animals on prolonged HFD feeding showed lipid accumulation in iBAT, the CGRPα⁻ mice exhibited healthy histological features despite prolonged HFD feeding (Figure 3A). After 15 weeks of DIO, the brown fat of the CGRPα⁻ mice had a striking reduction in the number of fat vacuoles
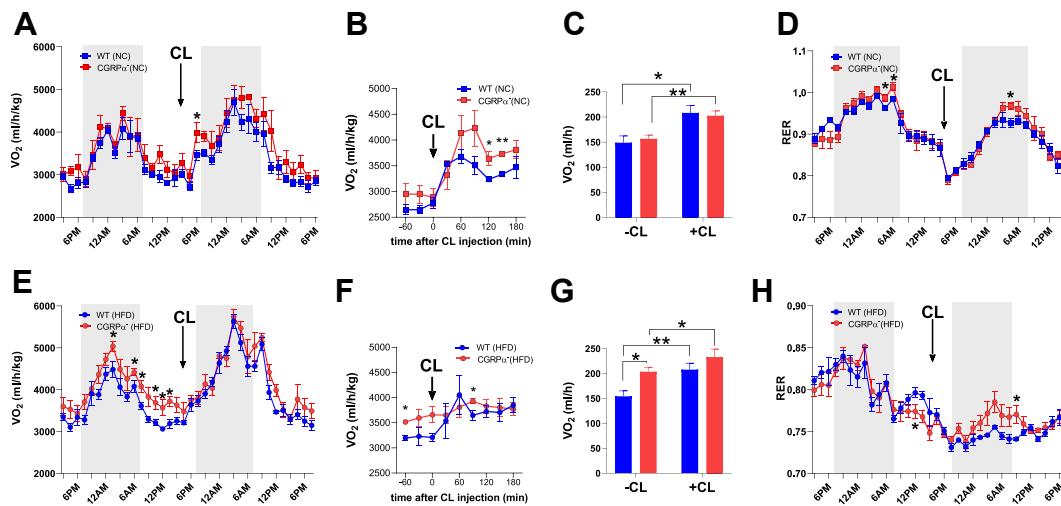
Figure 2: Loss of CGRPα neurons resulted in higher energy expenditure on high-fat diet feeding. (A) VO₂ in NC-fed animals before and after injection of the β-3 adrenergic agonist CL316,243 (CL). (B) Immediate response to CL monitored over 3 h. (C) Peak VO₂ values of the dark cycle obtained pre- and post-injection of CL. (D) RER in NC-fed animals before and after injection of CL. (E) VO₂ in HFD-fed animals on DIO for 2 weeks pre- and post-injection of CL. (F) Immediate response to CL monitored over 3 h. (G) Peak VO₂ values of the dark cycle obtained before and after CL delivery. (H) RER in HFD-fed animals before and after injection of CL. N = 5, **p < 0.001, and *p < 0.05. All of the values denote means ± SEM.
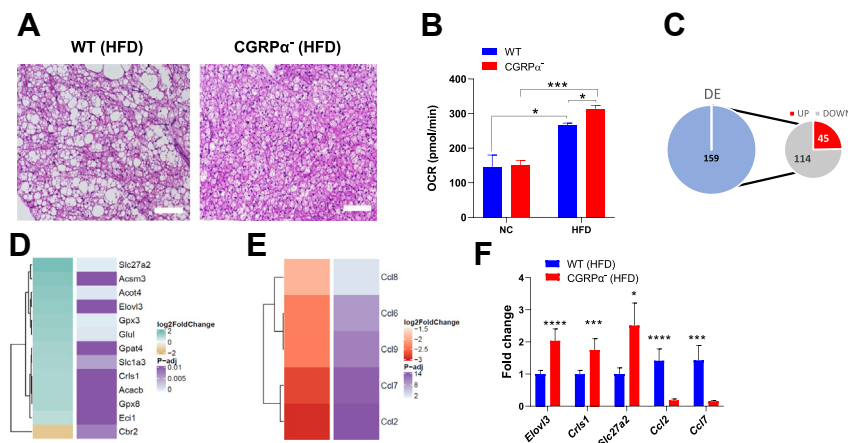

Figure 3: Increased lipid utilization in iBAT of the mice lacking CGRPα neurons. (A) Hematoxylin and eosin staining of iBAT from the HFD-fed CGRPα⁻ and WT controls littermates after 17 weeks of DIO. Scale bar 40 μm. (B) Basal oxygen consumption rate (OCR) of brown fat explants collected from the NC and HFD-fed mice measured by XF-Seahorse analyzer (N = 5). (C) Differential gene expression between the HFD-fed CGRPα⁻ and WT controls showing the distribution of shortlisted genes (p adj < 0.05, log₂ fold change > 0.7 or < −0.7, N = 4). (D and E) Heat maps representing differentially expressed genes in iBAT involved in fat metabolism, thermogenesis (D), and inflammatory chemokines (E) between HFD CGRPα⁻ and WT. (F) RT-qPCR validation of the differentially expressed genes (N = 6). ****p < 0.0001, ***p < 0.0001, **p < 0.001, and *p < 0.05. All of the values denote means ± SEM.

(Figure 3A). Lipid is stored in BAT as an essential proximal reservoir for fuel in response to adrenergically stimulated thermogenesis [2], therefore suggesting that lipolysis may be increased in mice lacking CGRPα neurons. In particular, the RER of the HFD-CGRPα⁻ was lower during the light cycle preceding CL treatment, consistent with increased FFA oxidation. Analysis of mitochondrial respiration in iBAT biopsies from the NC and HFD animals revealed a higher oxygen consumption rate (OCR) on the HFD vs the NC-fed mice, with a gain in mitochondrial respiration in the HFD-CGRPα⁻ mice compared to HFD-WT (Figure 3B). To further explore the mechanism behind higher energy expenditure phenotype in the CGRPα⁻ animals, we employed mRNA-seq to gain insight into changes in the BAT transcriptome of the HFD-fed animals. Using a stringent criterion (p adj < 0.05, log2

change > 0.7 or < −0.7, and base mean for genes across all of the samples > 100), we identified a list of 159 genes that were differentially expressed with 114 downregulated and 45 upregulated genes (Figure 3C). To derive a physiological interpretation of these changes, we subjected these shortlisted genes to the KEGG pathway analysis [24]. FFA metabolism was upregulated in the CGRPα⁻ samples, whereas chemokine signaling pathways were repressed (Figure 3D,E). We found 13 genes that were differentially expressed between genotypes and involved in FFA metabolism according to the KEGG analysis (Figure 3D). Interestingly, among the upregulated genes, we found genes that play a critical function in the induction and sustenance of a thermogenic program (*Crls1* and *Elovl3*). *Crls1* encodes for cardiolipin synthase and has been shown to be a master regulator of

thermogenesis in brown adipocytes [39]. We also found that the most significantly upregulated genes were part of the β-oxidation pathway (*Eci1*, *Acsm3*, and *Acot4*). Transcript levels of *Slc27a2*, a transporter involved in the cellular uptake of long-chain FFAs, were induced by three-fold (Figure 3F). Additionally, consistent with decreased inflammation and resistance to DIO, we found reduced expression of genes encoding chemokines in BAT in the CGRPα⁻ mice compared to WT (Figure 3F).

Surprisingly, the subcutaneous inguinal adipose tissue (iWAT) did not exhibit features of "browning," a typical phenomenon occurring upon long-term cold stress or chronic β3AR chemical activation [40]. Beige fat is characterized by the appearance of multilocular adipocytes expressing *Ucp1*, which uncouples mitochondrial oxidative phosphorylation from ATP production and dissipates energy as heat [41,42]. We did not observe higher transcriptional regulation of *Ucp1* in iWAT and iBAT arising from HFD-fed CGRPα⁻ mice after 15 weeks of DIO or upon acute CL treatment (Figure 4C,D). However, iWAT adipocytes appeared smaller in the CGRPα⁻ mice despite HFD feeding (Supp. Fig. 3b). We also performed mRNA sequencing on iWAT collected from the animals after 15 weeks of HFD treatment. Using similar criteria as for the iBAT analysis, we identified a list of 253 genes that were differentially expressed, with 172 genes downregulated and 81 upregulated (Supp. Fig. 3c). The KEGG pathway analysis revealed that adrenergic signaling pathway was induced (Supp. Fig. 3d). Peroxisome proliferator-activated receptor (PPAR) signaling was also stimulated, consistent with higher carbohydrate and lipid metabolism in the HFD-CGRPα⁻ mice. These data demonstrated that loss of CGRPα sensory neurons led to increased lipid utilization in iBAT without promoting browning of subcutaneous adipose tissue. Remarkably, this effect was sufficient to drive enhanced thermogenesis and ample weight loss on DIO (Figures 1B and 2E).

3.4. Improved fatty acid oxidation in white adipose tissue of mice lacking CGRPα neurons

Excessive calories stored in fat can be utilized by the activation of lipases capable of converting large lipid stores into triglycerides. Lipolysis in WAT is regulated by SNS release of catecholamines and β3AR stimulation of lipase activity [36,43]. Our results strongly suggested that lipolytic processes may be highly stimulated upon loss of CGRPα sensory innervation. To directly test this hypothesis, we evaluated the gonadal WAT (gWAT) histological profile. We observed that the HFD-CGRPα⁻ mice were protected against adipocyte hypertrophy in gWAT (Figure 4A). Gene expression analysis of the HFD-CGRPα⁻ mice also revealed a higher abundance of transcripts involved in FFA oxidative metabolism than HFD-WT (Supp. Fig. 4a).

Remarkably, CL treatment in the HFD-fed mice led to a robust upregulation of FAO genes, which was similar among the CL-treated WT and CGRPα⁻ mice. *Adrb3* (encoding β3-AR) transcript levels were elevated in the vehicle-treated HFD-CGRPα⁻ mice compared to WT, suggesting a higher recruitment of β3 adrenergic signaling in gWAT. In particular, *Adrb3* levels were indistinguishable from WT in iWAT and iBAT (Figure 4C,D). In accordance with no browning of adipose tissue, we did not observe transcriptional changes in *Ucp1*, *Prdm16*, *Cidea*, or genes encoding mitochondrial electron transport chain proteins in iWAT or iBAT (Figure 4C,D).

As our results point toward increased FFA oxidative metabolism in adipose tissue upon loss of CGRPα, we measured isoproterenol-induced lipolysis in biopsies from gWAT of the HFD-fed mice using established procedures [29]. Isoproterenol is an agonist of β-adrenergic receptors, the activation of which leads to lipase-dependent breakdown of cellular triglycerides. Consistent with our FAO gene

expression and low RER during the sleep phase, we found that the lipolysis rate increased in the HFD-CGRPα⁻ animals (Figure 4E). However, acute CL treatment a week before tissue collection led to an initial burst in lipolysis (t0) but blunted the effects of CGRP neuron ablation on adipocytes (Figure 4F).

We also investigated whether loss of CGRPα neurons could alter the content of sympathetic nerves releasing NE in gWAT. As several studies have reported that sympathetic axons can undergo profound neural density changes when animals are exposed to prolonged cold environments [44,45], we quantified the protein content of tyrosine hydroxylase (TH) in the HFD-fed animals. The TH content remained similar among the genotypes after 6 weeks of HFD treatment in both gWAT and iWAT (Supp. Fig. 4b ,c). This result suggested that loss of CGRPα neurons did not directly cause changes in SNS innervation content but could alter SNS activity by promoting increased β-adrenergic signaling and FAO in gonadal WAT.

3.5. Loss of CGRPα neurons induced tail vasoconstriction at room temperature

In response to cold, the CNS triggers an array of counter-regulatory responses to conserve heat in the body. These responses are cutaneous vasoconstriction, piloerection, and heat production through thermogenesis [1]. Remarkably, mice lacking CGRPα neurons have been reported to display exacerbated cold perception and reduced ability to normalize their core temperature after skin cooling [21]. We therefore asked if the increased energy expenditure and higher FFA metabolism of these mice was associated with increased sensory response to lower temperatures. Importantly, the CGRPα⁻ animals were able to regulate their core temperature upon a 5 h-cold stress challenge (Supp. Fig. 5a). We then examined the thermogenic profile of these mice during "mild cold stress" caused by the housing temperature (22 °C) and a warmer environment considered to be thermoneutral (28 °C). We measured the rectal core temperature, iBAT, and tail temperature using infrared thermal imaging to respectively determine BAT thermogenic response and tail vasoconstriction.

Core body temperature appeared similar among the genotypes on the NC diet (Supp. Fig. 5b and c). As the tail is a major source of heat loss in mice, vasoconstriction in that area is highly regulated [46]. At 22 °C, the tails of the CGRPα⁻ animals on both the NC and HFD were significantly colder, suggesting higher vasoconstriction (Figure 5A-C). Thermoneutrality mostly restored the tail temperature of all of the mice on the NC (Figure 5D), but the HFD-CGRPα⁻ animals manifested colder tail temperatures during the night cycle (Figure 5E,F). This inability to perform vasodilation specifically on the HFD was associated with reduced core temperature during the night cycle (Supp. Fig. 5e). This result suggested that that deletion of CGRPα neurons led to thermoregulatory deficiencies during HFD-induced thermogenesis.

Because of the increased vasoconstriction of tail blood vessels in mice lacking CGRPα neurons, we also evaluated if iBAT temperature increased in these mice as part of a counter-regulatory response stimulating adaptive thermogenesis. At 22 °C, the iBAT temperature was increased during the night cycle in the CGRPα⁻ mice (Figure 5G) and further increased to 28 °C (Figure 5H). Remarkably, these results suggested that the CGRPα⁻ mice "felt" cold at thermoneutrality when placed on the HFD. Counter-regulatory responses to drive adaptive thermogenesis were engaged but did not fully restore their core temperature to normal levels (Figure 5E,H and Supp. Fig. 5e). These results suggested that the HFD led to enhanced cold perception in the CGRPα⁻ animals and drove iBAT thermogenesis.

To address whether the CGRPα⁻ animals were also more responsive to cooling-dependent thermogenesis, we used the TRPM8 agonist
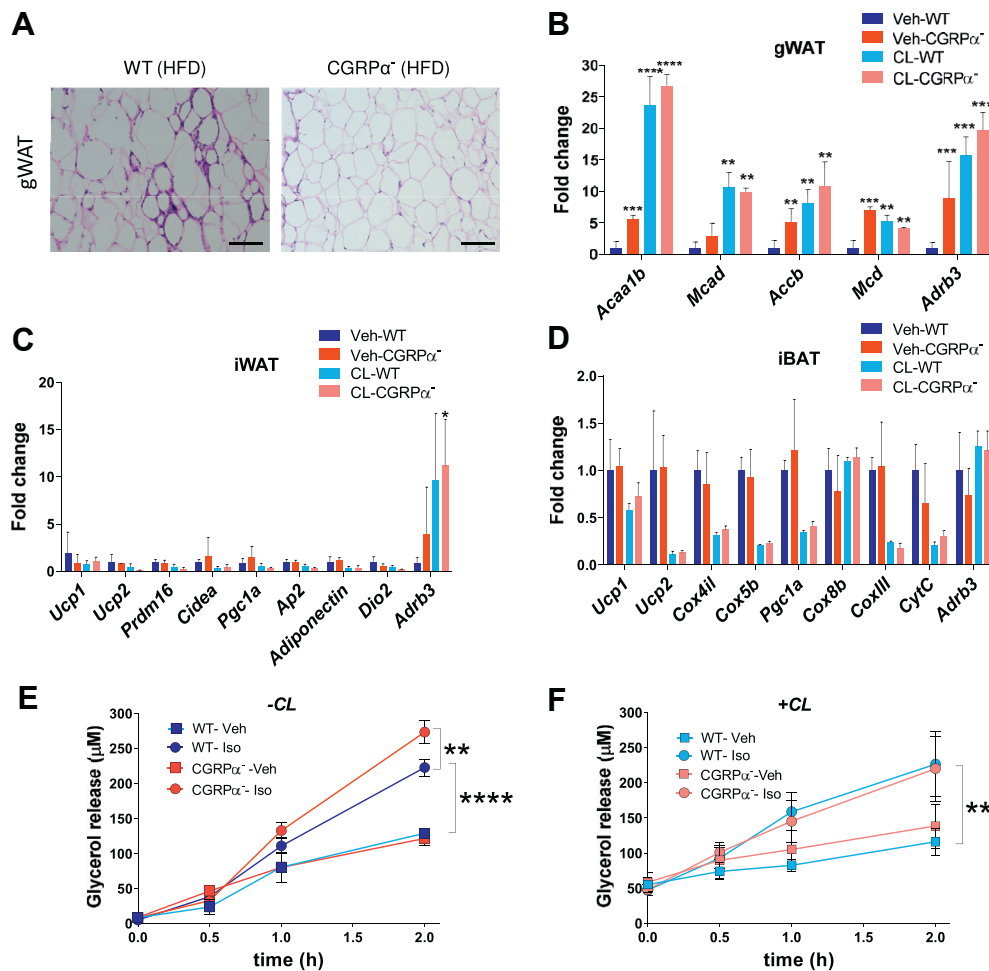
Figure 4: Higher energy expenditure of the CGRPα⁻ mice was linked with increased fatty acid utilization in white adipose tissue. (A) Hematoxylin and eosin staining of gonadal WAT from littermates after 17 weeks of DIO. Scale bar 60 μm. (B–D) RT-qPCR of fatty acid oxidation genes in gonadal WAT (B), inguinal WAT (C), and intrascapular BAT collected from the HFD-fed mice treated with acute CL injection (1 mg/kg) or vehicle (Saline). (E) *Exvivo* lipolysis in gWAT biopsies treated with vehicle (Veh) or isoproterenol (Iso) in the HFD-fed mice that received acute vehicle (Saline) injections a week prior to sacrifice. (F) *Exvivo* lipolysis in gWAT biopsies treated with vehicle (Veh) or isoproterenol (Iso) in the HFD-fed mice that received acute CL injections a week prior to sacrifice. N = 5−6, ****p < 0.0001, ***p < 0.0001, **p < 0.001, and *p < 0.05. All of the values denote means ± SEM.

icilin, which mimics the metabolic effects of acute cold exposure [47]. Acute injection of icilin (0.6 mg/kg) produces a potent TRPM8-dependent cooling sensation and a concomitant burst in energy expenditure without increasing Ucp1 mRNA levels in adipocytes [47]. Administration of icilin drove an immediate tail-cooling response in the NC-fed WT and CGRPα⁻ animals (Supp. Fig. 5f) characterized by an increased iBAT thermogenic profile in the CGRPα⁻ animals within the 60 min following injection (Figure 5I). Thus, both cooling and HFD promoted iBAT adaptive thermogenesis upon loss of heat-sensing CGRPα neurons.

3.6. BAT specific loss of CGRPα neurons did not contribute to higher energy expenditure

Strikingly, our results demonstrated that loss of CGRPα sensory innervation was associated with higher BAT thermogenesis on the HFD. This finding raises the important question to determine whether the sensory detection of temperature occurs within adipose tissue itself. Rat iBAT contains significant sensory innervation of substance P- and CGRP-immunoreactive nerve fibers within the parenchyma and vasculature areas [48—50]. We therefore investigated the extent of

CGRPα and SNS neuronal innervation in different adipose tissues including iBAT, iWAT, and gWAT using tissue-clearing techniques [25]. Adipo-Clear was used to generate three-dimensional innervation patterns of adipose tissues from the NC-fed CGRPα-GFP and WT mice. We assessed the CGRPα-GFP presence in iBAT and observed discrete fibers mostly associated with TH fibers (Figure 6A). However, in gWAT and iWAT, sparse CGRPα (green) neurons were detected in nerve bundles with overlay with TH fibers (magenta) or tissue parenchyma of iWAT (Supp. Fig. 6B and C).

In previous attempts to connect sensory innervation with mechanisms of BAT adaptive thermogenesis, injection of capsaicin directly in iBAT of Siberian hamsters led to reduced iBAT temperatures at 4 and 22 °C [51]. However, whether this high capsaicin dosage successfully ablated the TRPV1 neurons in this tissue remains unclear. Because we observed the presence of sensory CGRPα-GFP in iBAT and a thermogenic phenotype upon loss of CGRPα neurons, we investigated the role of the CGRPα fibers present in iBAT. Changes in iBAT temperature could potentially be detected locally by sensory neurons to rapidly mount counter-regulatory responses through the CNS. We therefore specifically ablated iBAT-CGRPα neurons by local DT microinjections in
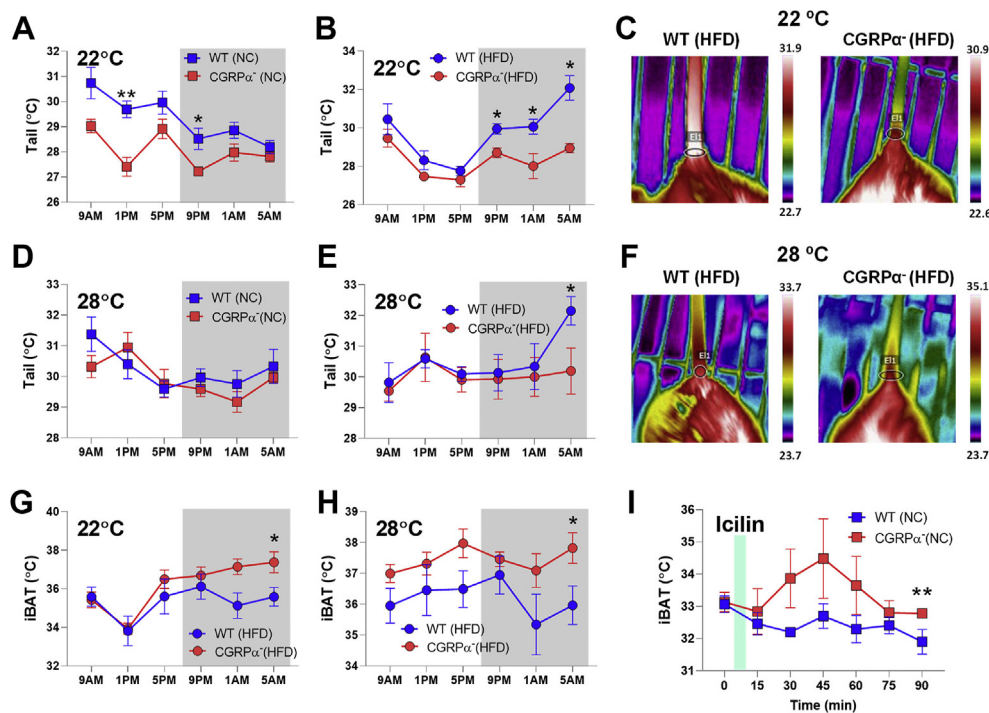
Figure 5: Loss of CGRPα neurons resulted in tail vasoconstriction and increased iBAT temperature on the high-fat diet. (A and B) Infrared imaging of tail temperatures at room temperature (22 °C) in (A) the NC-fed mice and (B) HFD-fed mice. (C) Representative images of dark cycle tail recordings from the HFD-fed mice at 22 °C. (D and E) Tail temperature recordings at thermoneutrality (28 °C) in the NC-fed (D) and HFD-fed (E) mice. (F) Representative images of dark cycle tail recordings from the HFD-fed mice at 28 °C. (G—H) Cutaneous iBAT temperature at 22 °C (G) and 28 °C (H) in the HFD-fed mice. (I) Infrared imaging of iBAT in the NC-fed mice upon administration of icilin (0.6 mg/kg). N = 5, **p < 0.001, and *p < 0.05. All of the values denote means ± SEM.

both iBAT fat pads of the CGRPα⁻ mice, which were also administered to their control littermates (iBAT-sham). Hot plate assays were used to verify the absence of generalized sensory ablation beyond iBAT. As expected, both groups responded similarly in their paw withdrawal reflex at 52 °C (Supp. Fig. 6c). We also verified the ablation of CGRPα-GFP neurons in iBAT (Supp. Fig. 6d).

We then subjected the iBAT-CGRPα⁻ and control iBAT-sham mice to DIO. Remarkably, the iBAT-CGRPα⁻ animals gained weight to a similar extent as the controls (Figure 6B) and had similar fat and lean mass (Figure 6C). There was no difference in VO₂ in both genotypes, with a trend toward lower energy expenditure in the iBAT-CGRPα⁻ mice (Figure 6D), whereas food intake and activity remained unchanged (Figure 6E and Supp. Fig. 6e). Tail, body core, and iBAT temperatures remained similar to the controls upon loss of CGRPα neurons in iBAT (Figure 6F-H). Taken together, these findings suggested that sensory innervation within iBAT is dispensable for the detection of temperature signals and regulation of energy metabolism in response to HFD-induced thermogenesis.

4. DISCUSSION

In mammals, the capacity to integrate information about the external milieu and constantly optimize adaptation to changing environments is driven by a multitude of pseudounipolar neurons projecting to the DRG in the peripheral nervous system [3,4,52]. These sensory fibers densely innervate the skin where they detect changes in temperature before informing the CNS [53—55]. Although it has been established that non-shivering thermogenesis depends on sensory detection of the environment, the role of sensory neurons responsible for this function is poorly understood. The results presented herein provide evidence

that loss of CGRPα neurons increases cutaneous vasoconstriction and cold perception at room temperature, therefore promoting a higher metabolic rate and resistance to DIO.

Given the existing precedents linking TRPV1 to energy metabolism [14,17,18,56], we characterized the role of sensory thermoreceptor neurons expressing CGRPα upon DIO. Using a selective method to ablate these neurons in adult animals, we found that loss of CGRPα sensory neurons dramatically reduced weight gain on HFD feeding by increasing energy expenditure (Figures 1 and 2). Removal of CGRPα neurons led to similar weight-loss benefits on HFD than genetic mutation of the TRPV1 receptor, suggesting that peptidergic TRPV1 neurons largely account for the metabolic effects associated with manipulation of this ion channel and associated sensory neurons [14,17,57,58].

How do the CGRPα sensory neurons regulate energy homeostasis? Interestingly, much evidence links TRPV1 to alterations in core temperature [51,59,60], arguing that this ion channel can both sense external temperature and modulate CNS-dependent adjustments of homeostasis. Cutaneous thermoreceptor neurons from the DRG express high levels of TRPV1 to detect changes in skin temperature and contribute to counter-regulatory responses to keep core temperature at a steady level. McCoy et al. demonstrated that half of the sensory neurons containing TRPV1 are peptidergic and encode for CGRPα [10]. These neurons play a fundamental role in thermoregulation by tonically inhibiting TRPM8 cold-sensing afferent DRG neurons at the level of the spinal cord [21]. Therefore, loss of CGRPα neurons leads to higher perception of cooling stimuli [21]. We further characterized the thermogenic response of mice lacking CGRPα neurons in response to the ambient temperature, which was below thermoneutral conditions for mice and constituted a sustained cold stress [61]. Our data
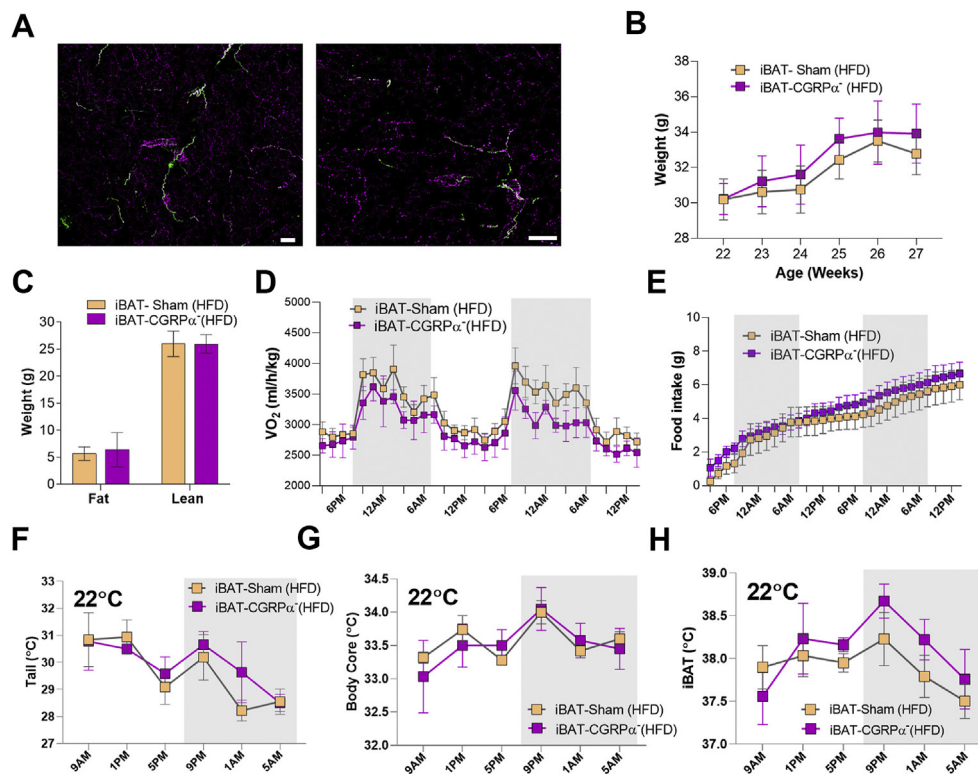
Figure 6: Intrascapular BAT-specific deletion of CGRPα neurons did not regulate energy metabolism and tail vasoconstriction. (A) Immunostaining of GFP (green) and TH (magenta) in cleared iBAT sections isolated from the $Calca^{-<lox-GFP-lox-hDTR>}$ mice on NC showing CGRPα-GFP nerves lining TH$^+$ fibers in the vasculature. Left panel (scale 50 μm) and right panel (scale 40 μm). (B) Weight gain of 22-week-old mice placed on the HFD after receiving DT microinjections in iBAT. (C) Fat mass and lean mass after 5 weeks of DIO. (D and E) VO$_2$ (D) and food intake (E) measurements obtained 4 weeks after switching the mice to DIO. (F—H) Infrared imaging of tail temperatures (F), rectal probe measurement of body core temperatures (G), and infrared imaging of iBAT (H) obtained at room temperature (22 °C) in the HFD-fed iBAT-DT mice.

demonstrated a sustained reduction in tail temperature, suggesting the induction of a vasoconstrictive response (Figure 5). We then used this exacerbated cold response to understand the role of thermoreceptors in adipose thermogenesis and asked whether the animals would exhibit higher thermogenic responses to dietary changes. Our data showed that lipid utilization mechanisms were strongly engaged in response to DIO and translated into an enhanced energy expenditure phenotype allowing the CGRPα$^-$ mice to remain leaner despite consumption of a HFD.

To maintain body temperature against cold environments, the CNS orchestrates effector responses controlling cutaneous vasoconstriction, piloerection to reduce skin heat loss, shivering, and BAT thermogenesis [1]. Our results are consistent with a model in which loss of CGRPα neurons drives a cold defense metabolic program to raise the core body temperature through counter-regulatory mechanisms. In accordance with this hypothesis, CGRPα DRG neuronal denervation led to increased adaptive thermogenesis in iBAT during HFD feeding (Figures 3 and 5). This thermogenic response also involved exacerbated lipolysis in gWAT (Figure 4). Consistent with a well-characterized recruitment of β3-adrenergic signaling in WAT to promote lipolysis and fatty acid oxidation [62—65], we observed increased mRNA levels of *Adrb3* in this tissue (Figure 4B) and higher immediate CL-dependent oxygen consumption in the mice lacking CGRPα neurons (Figure 2B,F). In this model, loss of CGRPα neurons in the skin activates a "cold-sensing" neurocircuit that results in enhanced cutaneous vasoconstriction and adaptive thermogenesis to maintain core temperature. In the present study, we did not investigate how these signals propagate within the preoptic area and dorsomedial hypothalamus,

two hypothalamic areas that have been shown to participate in activating cold-induced counter-regulatory responses [1]. It is, however, highly plausible that increased CNS counter-regulatory responses were engaged upon loss of the CGRPα sensory nerves due to mild cold stress caused by housing temperatures. This CNS "impaired interpretation" occurred on both HFD and NC as observed by tail vasoconstriction responses (Figure 5A,B). However, the metabolic benefits were only observed on the HFD, most likely due to increased ability of the CGRPα$^-$ animals to burn calories through enhanced diet-induced thermogenesis. Increased sympathetic outflow to BAT, determining BAT thermogenesis, is controlled by central mechanisms in response to integration of sensory perception such as prolonged skin cooling [1]. Our results were consistent with exacerbated cold perception in CGRPα$^-$ mice at housing temperatures, leading to recruitment of BAT thermogenesis through CNS-dependent integration of these sensory stimuli.

In response to higher temperatures, excitation of TRPV1 sensory neurons may release peptidergic signals to cutaneous blood vessels, with CGRPα being the predominant neuropeptide secreted and a potent vasodilator [66]. Innervation of blood vessels by perivascular sensory nerves containing CGRPα allows local peptide release to directly control vessel dilation in addition to central effector pathways [67]. Remarkably, CGRP-positive perivascular nerves innervate mostly small blood vessels and are weakly present around epicardial coronary veins of the heart [68,69]. CGRPα levels increase with conditions associated with weight gain including obesity, pregnancy, and aging [13,17,67,70]. Interventions resulting in decreased levels of circulatory CGRPα levels have proven efficient at increasing energy expenditure

and ameliorating weight loss [17,56,71]. The removal of CGRPα nerves achieved in our study is likely to strongly impair perivascular release of this neuropeptide and cause a steep decline in circulating CGRPα levels [72]. We recently showed that monoclonal antibody treatment against CGRPα enhanced energy expenditure and weight loss in diabetic mice [73]. These results were in line with our observation that loss of the CGRPα neurons stimulates cutaneous vasoconstriction and increases energy expenditure, leading to reduced weight gain during HFD feeding. In this model, CGRPα neurons and associated CGRPα peptide work together in a warm environment to 1) tonically inhibit TRPM8 neurons, 2) secrete CGRPα to elicit vasodilation and decrease metabolic rates, and 3) send afferent responses to the CNS to reduce sympathetic outflow to BAT and lower thermogenesis. Thus, loss of these neurons would maintain the body in high metabolic activity and enhance thermogenesis under mild cold stress.

5. CONCLUSIONS

Taken together, our findings illustrated that cutaneous thermoreceptors expressing CGRPα play a major role in vasodilation, thermoregulation, and diet-dependent thermogenesis. Perturbations in cold-sensing neurocircuits have the potential to promote weight-loss programs by stimulating cutaneous vasoconstriction and increasing lipolysis. In particular, we showed that CGRPα sensory neurons, by inhibiting thermogenesis, are a potential target for obesity and weight loss.

AUTHOR CONTRIBUTIONS

KM, HC, NM, EN, PTN, YW, PJ, and CER conducted the *invivo* experiments. JC, WB, and PC performed immunostaining of adipose tissue. CER designed the study and wrote the manuscript.

CONFLICT OF INTEREST

None declared.

APPENDIX A. SUPPLEMENTARY DATA

Supplementary data to this article can be found online at https://doi.org/10.1016/j.molmet.2021.101161.

REFERENCES

[1] Morrison, S.F., 2016. Central neural control of thermoregulation and brown adipose tissue. Autonomic Neuroscience: Basic & Clinical 196:14—24. https://doi.org/10.1016/j.autneu.2016.02.010.

[2] Betz, M.J., Enerbäck, S., 2018. Targeting thermogenesis in brown fat and muscle to treat obesity and metabolic disease. Nature Reviews Endocrinology 14(2):77—87. https://doi.org/10.1038/nrendo.2017.132.

[3] Bartness, T.J., Song, C.K., 2007. Thematic review series: adipocyte biology. Sympathetic and sensory innervation of white adipose tissue. Journal of Lipid Research 48(8):1655—1672. https://doi.org/10.1194/jlr.R700006-JLR200.

[4] Marino, J.S., Xu, Y., Hill, J.W., 2011. Central insulin and leptin-mediated autonomic control of glucose homeostasis. Trends in Endocrinology and Metabolism: Trends in Endocrinology and Metabolism 22(7):275—285. https://doi.org/10.1016/j.tem.2011.03.001.

[5] Caterina, M.J., Schumacher, M.A., Tominaga, M., Rosen, T.A., Levine, J.D., Julius, D., 1997. The capsaicin receptor: a heat-activated ion channel in the pain pathway. Nature 389(6653):816—824. https://doi.org/10.1038/39807.

[6] Caterina, M.J., Leffler, A., Malmberg, A.B., Martin, W.J., Trafton, J., Petersen-Zeitz, K.R., et al., 2000. Impaired nociception and pain sensation in mice lacking the capsaicin receptor. Science 288(5464):306—313. https://doi.org/10.1126/science.288.5464.306.

[7] Bautista, D.M., Siemens, J., Glazer, J.M., Tsuruda, P.R., Basbaum, A.I., Stucky, C.L., et al., 2007. The menthol receptor TRPM8 is the principal detector of environmental cold. Nature 448(7150):204—208. https://doi.org/10.1038/nature05910.

[8] Dhaka, A., Murray, A.N., Mathur, J., Earley, T.J., Petrus, M.J., Patapoutian, A., 2007. TRPM8 is required for cold sensation in mice. Neuron 54(3):371—378. https://doi.org/10.1016/j.neuron.2007.02.024.

[9] Patapoutian, A., Peier, A.M., Story, G.M., Viswanath, V., 2003. ThermoTRP channels and beyond: mechanisms of temperature sensation. Nature Reviews Neuroscience 4(7):529—539. https://doi.org/10.1038/nrn1141.

[10] McCoy, E.S., Taylor-Blake, B., Zylka, M.J., 2012. Cgrpα-expressing sensory neurons respond to stimuli that evoke sensations of pain and itch. PloS One 7(5):e36355. https://doi.org/10.1371/journal.pone.0036355.

[11] Kawabata, F., Inoue, N., Yazawa, S., Kawada, T., Inoue, K., Fushiki, T., 2006. Effects of CH-19 sweet, a non-pungent cultivar of red pepper, in decreasing the body weight and suppressing body fat accumulation by sympathetic nerve activation in humans. Bioscience, Biotechnology, and Biochemistry 70(12): 2824—2835. https://doi.org/10.1271/bbb.60206.

[12] Kawada, T., Sakabe, S., Watanabe, T., Yamamoto, M., Iwai, K., 1988. Some pungent principles of spices cause the adrenal medulla to secrete catecholamine in anesthetized rats. Proceedings of the Society for Experimental Biology and Medicine. Society for Experimental Biology and Medicine (New York, N.Y.) 188(2):229—233.

[13] Melnyk, A., Himms-Hagen, J., 1995. Resistance to aging-associated obesity in capsaicin-desensitized rats one year after treatment. Obesity Research 3(4): 337—344.

[14] Motter, A.L., Ahern, G.P., 2008. TRPV1-null mice are protected from diet-induced obesity. FEBS Letters 582(15):2257—2262. https://doi.org/10.1016/j.febslet.2008.05.021.

[15] Ono, K., Tsukamoto-Yasui, M., Hara-Kimura, Y., Inoue, N., Nogusa, Y., Okabe, Y., et al., 2011. Intragastric administration of capsiate, a transient receptor potential channel agonist, triggers thermogenic sympathetic responses. Journal of Applied Physiology (Bethesda, Md.: 1985) 110(3):789—798. https://doi.org/10.1152/japplphysiol.00128.2010.

[16] Westerterp-Plantenga, M.S., Smeets, A., Lejeune, M.P.G., 2005. Sensory and gastrointestinal satiety effects of capsaicin on food intake. International Journal of Obesity 29(6):682—688. https://doi.org/10.1038/sj.ijo.0802862, 2005.

[17] Riera, C.E., Huising, M.O., Follett, P., Leblanc, M., Halloran, J., Van Andel, R., et al., 2014. TRPV1 pain receptors regulate longevity and metabolism by neuropeptide signaling. Cell 157(5):1023—1036. https://doi.org/10.1016/j.cell.2014.03.051.

[18] Jeong, J.H., Lee, D.K., Liu Jr., S.-M., S, C.C., Schwartz, G.J., Jo, Y.-H., 2018. Activation of temperature-sensitive TRPV1-like receptors in ARC POMC neurons reduces food intake. PLoS Biology 16(4):e2004399. https://doi.org/10.1371/journal.pbio.2004399.

[19] Bachman, E.S., Dhillon, H., Zhang, C.-Y., Cinti, S., Bianco, A.C., Kobilka, B.K., et al., 2002. βAR signaling required for diet-induced thermogenesis and obesity resistance. Science 297(5582):843—845. https://doi.org/10.1126/science.1073160.

[20] Lowell, B.B., Bachman, E.S., 2003. Beta-Adrenergic receptors, diet-induced thermogenesis, and obesity. Journal of Biological Chemistry 278(32): 29385—29388. https://doi.org/10.1074/jbc.R300011200.

[21] McCoy, E.S., Taylor-Blake, B., Street, S.E., Pribisko, A.L., Zheng, J., Zylka, M.J., 2013. Peptidergic CGRPα primary sensory neurons encode heat and itch and tonically suppress sensitivity to cold. Neuron 78(1):138—151. https://doi.org/10.1016/j.neuron.2013.01.030.

[22] Dobin, A., Davis, C.A., Schlesinger, F., Drenkow, J., Zaleski, C., Jha, S., et al., 2013. STAR: ultrafast universal RNA-seq aligner. Bioinformatics (Oxford, England) 29(1):15—21. https://doi.org/10.1093/bioinformatics/bts635.

[23] Love, M.I., Huber, W., Anders, S., 2014. Moderated estimation of fold change and dispersion for RNA-seq data with DESeq2. Genome Biology 15(12):550. https://doi.org/10.1186/s13059-014-0550-8.

[24] Huang, D.W., Sherman, B.T., Lempicki, R.A., 2009. Systematic and integrative analysis of large gene lists using DAVID bioinformatics resources. Nature Protocols 4(1):44—57. https://doi.org/10.1038/nprot.2008.211.

[25] Chi, J., Crane, A., Wu, Z., Cohen, P., 2018. Adipo-clear: a tissue clearing method for three-dimensional imaging of adipose tissue. Journal of Visualized Experiments(137):e58271. https://doi.org/10.3791/58271.

[26] Hasegawa, H., Abbott, S., Han, B.-X., Qi, Y., Wang, F., 2007. Analyzing somatosensory axon projections with the sensory neuron-specific Advillin gene. Journal of Neuroscience: The Official Journal of the Society for Neuroscience 27(52):14404—14414. https://doi.org/10.1523/JNEUROSCI.4908-07.2007.

[27] Chen, J.Y., Campos, C.A., Jarvie, B.C., Palmiter, R.D., 2018. Parabrachial CGRP neurons establish and sustain aversive taste memories. Neuron 100(4): 891—899. https://doi.org/10.1016/j.neuron.2018.09.032 e5.

[28] Han, S., Soleiman, M.T., Soden, M.E., Zweifel, L.S., Palmiter, R.D., 2015. Elucidating an affective pain circuit that creates a threat memory. Cell 162(2): 363—374. https://doi.org/10.1016/j.cell.2015.05.057.

[29] Riera, C.E., Tsaousidou, E., Halloran, J., Follett, P., Hahn, O., Pereira, M.M.A., et al., 2017. The sense of smell impacts metabolic health and obesity. Cell Metabolism 26(1):198—211. https://doi.org/10.1016/j.cmet.2017.06.015 e5.

[30] Collins, S., 2012. β-Adrenoceptor signaling networks in adipocytes for recruiting stored fat and energy expenditure. Frontiers in Endocrinology 2. https://doi.org/10.3389/fendo.2011.00102.

[31] Nahmias, C., Blin, N., Elalouf, J.M., Mattei, M.G., Strosberg, A.D., Emorine, L.J., 1991. Molecular characterization of the mouse beta 3-adrenergic receptor: relationship with the atypical receptor of adipocytes. The EMBO Journal 10(12):3721—3727.

[32] Arch, J.R.S., Ainsworth, A.T., Cawthorne, M.A., Piercy, V., Sennitt, M.V., Thody, V.E., et al., 1984. Atypical β-adrenoceptor on brown adipocytes as target for anti-obesity drugs. Nature 309:163—165. https://doi.org/10.1038/309163a0.

[33] Chouchani, E.T., Kazak, L., Spiegelman, B.M., 2019. New advances in adaptive thermogenesis: UCP1 and beyond. Cell Metabolism 29(1):27—37. https://doi.org/10.1016/j.cmet.2018.11.002.

[34] Kazak, L., Chouchani, E.T., Jedrychowski, M.P., Erickson, B.K., Shinoda, K., Cohen, P., et al., 2015. A creatine-driven substrate cycle enhances energy expenditure and thermogenesis in beige fat. Cell 163(3):643—655. https://doi.org/10.1016/j.cell.2015.09.035.

[35] Galmozzi, A., Sonne, S.B., Keylin, S., Hasegawa, Y., Shinoda, K., Luijten, I.H.N., et al., 2014. ThermoMouse: an in vivo model to identify modulators of UCP1 expression in brown adipose tissue. Cell Reports 9(5): 1584—1593. https://doi.org/10.1016/j.celrep.2014.10.066.

[36] MacPherson, R.E.K., Castellani, L., Beaudoin, M.-S., Wright, D.C., 2014. Evidence for fatty acids mediating CL 316,243-induced reductions in blood glucose in mice. American Journal of Physiology - Endocrinology and Metabolism 307(7):E563—E570. https://doi.org/10.1152/ajpendo.00287.2014.

[37] Atgié, C., Faintrenie, G., Carpéné, C., Bukowiecki, L.J., Géloën, A., 1998. Effects of chronic treatment with noradrenaline or a specific β3-adrenergic agonist, CL 316 243, on energy expenditure and epididymal adipocyte lipolytic activity in rat. Comparative Biochemistry and Physiology Part A: Molecular & Integrative Physiology 119(2):629—636. https://doi.org/10.1016/S1095-6433(97)00476-5.

[38] Reilly, S.M., Hung, C.-W., Ahmadian, M., Zhao, P., Keinan, O., Gomez, A.V., et al., 2020. Catecholamines suppress fatty acid re-esterification and increase oxidation in white adipocytes via STAT3. Nature Metabolism 2(7):620—634. https://doi.org/10.1038/s42255-020-0217-6.

[39] Sustarsic, E.G., Ma, T., Lynes, M.D., Larsen, M., Karavaeva, I., Havelund, J.F., et al., 2018. Cardiolipin synthesis in Brown and beige fat mitochondria is essential for systemic energy homeostasis. Cell Metabolism 28(1):159—174. https://doi.org/10.1016/j.cmet.2018.05.003 e11.

[40] Cohen, P., Spiegelman, B.M., 2015. Brown and beige fat: molecular parts of a thermogenic machine. Diabetes 64(7):2346—2351. https://doi.org/10.2337/db15-0318.

[41] Kozak, L.P., Anunciado-Koza, R., 2008. UCP1: its involvement and utility in obesity. International Journal of Obesity 32(Suppl 7):S32—S38. https://doi.org/10.1038/ijo.2008.236, 2005.

[42] Enerbäck, S., Jacobsson, A., Simpson, E.M., Guerra, C., Yamashita, H., Harper, M.E., et al., 1997. Mice lacking mitochondrial uncoupling protein are cold-sensitive but not obese. Nature 387(6628):90—94. https://doi.org/10.1038/387090a0.

[43] Carmen, G.-Y., Víctor, S.-M., 2006. Signalling mechanisms regulating lipolysis. Cellular Signalling 18(4):401—408. https://doi.org/10.1016/j.cellsig.2005.08.009.

[44] Jiang, H., Ding, X., Cao, Y., Wang, H., Zeng, W., 2017. Dense intra-adipose sympathetic arborizations are essential for cold-induced beiging of mouse white adipose tissue. Cell Metabolism 26(4):686—692. https://doi.org/10.1016/j.cmet.2017.08.016 e3.

[45] Zeng, X., Ye, M., Resch, J.M., Jedrychowski, M.P., Hu, B., Lowell, B.B., et al., 2019. Innervation of thermogenic adipose tissue via a calsyntenin 3β-S100b axis. Nature 569(7755):229—235. https://doi.org/10.1038/s41586-019-1156-9.

[46] Reimúndez, A., Fernández-Peña, C., García, G., Fernández, R., Ordás, P., Gallego, R., et al., 2018. Deletion of the cold thermoreceptor TRPM8 increases heat loss and food intake leading to reduced body temperature and obesity in mice. Journal of Neuroscience 38(15):3643—3656. https://doi.org/10.1523/JNEUROSCI.3002-17.2018.

[47] Clemmensen, C., Jall, S., Kleinert, M., Quarta, C., Gruber, T., Reber, J., et al., 2018. Coordinated targeting of cold and nicotinic receptors synergistically improves obesity and type 2 diabetes. Nature Communications 9. https://doi.org/10.1038/s41467-018-06769-y.

[48] Ryu, V., Garretson, J.T., Liu, Y., Vaughan, C.H., Bartness, T.J., 2015. Brown adipose tissue has sympathetic-sensory feedback circuits. Journal of Neuroscience 35(5):2181—2190. https://doi.org/10.1523/JNEUROSCI.3306-14.2015.

[49] Norman, D., Mukherjee, S., Symons, D., Jung, R.T., Lever, J.D., 1988. Neuropeptides in interscapular and perirenal brown adipose tissue in the rat: a plurality of innervation. Journal of Neurocytology 17(3):305—311.

[50] Lever, J.D., Mukherjee, S., Norman, D., Symons, D., Jung, R.T., 1988. Neuropeptide and noradrenaline distributions in rat interscapular brown fat and in its intact and obstructed nerves of supply. Journal of the Autonomic Nervous System 25(1):15—25.

[51] Vaughan, C.H., Bartness, T.J., 2012. Anterograde transneuronal viral tract tracing reveals central sensory circuits from brown fat and sensory denervation alters its thermogenic responses. American Journal of Physiology -

Regulatory, Integrative and Comparative Physiology 302(9):R1049—R1058. https://doi.org/10.1152/ajpregu.00640.2011.

[52] Saito, M., Matsushita, M., Yoneshiro, T., Okamatsu-Ogura, Y., 2020. Brown adipose tissue, diet-induced thermogenesis, and thermogenic food ingredients: from mice to men. Frontiers in Endocrinology 11. https://doi.org/10.3389/fendo.2020.00222.

[53] Buck, S.H., Burks, T.F., 1986. The neuropharmacology of capsaicin: review of some recent observations. Pharmacological Reviews 38(3):179—226.

[54] Holzer, P., 1991. Capsaicin: cellular targets, mechanisms of action, and selectivity for thin sensory neurons. Pharmacological Reviews 43(2):143—201.

[55] Szallasi, A., Blumberg, P.M., 1999. Vanilloid (Capsaicin) receptors and mechanisms. Pharmacological Reviews 51(2):159—212.

[56] Gram, D.X., Hansen, A.J., Deacon, C.F., Brand, C.L., Ribel, U., Wilken, M., et al., 2005. Sensory nerve desensitization by resiniferatoxin improves glucose tolerance and increases insulin secretion in Zucker Diabetic Fatty rats and is associated with reduced plasma activity of dipeptidyl peptidase IV. European Journal of Pharmacology 509(2):211—217. https://doi.org/10.1016/j.ejphar.2004.12.039.

[57] Riera, C.E., Dillin, A., 2016. Emerging role of sensory perception in aging and metabolism. Trends in Endocrinology and Metabolism: Trends in Endocrinology and Metabolism 27(5):294—303. https://doi.org/10.1016/j.tem.2016.03.007.

[58] Ahern, G.P., 2013. Transient receptor potential channels and energy homeostasis. Trends in Endocrinology and Metabolism 24(11):554—560. https://doi.org/10.1016/j.tem.2013.06.005.

[59] Feketa, V.V., Balasubramanian, A., Flores, C.M., Player, M.R., Marrelli, S.P., 2013. Shivering and tachycardic responses to external cooling in mice are substantially suppressed by TRPV1 activation but not by TRPM8 inhibition. American Journal of Physiology - Regulatory, Integrative and Comparative Physiology 305(9):R1040—R1050. https://doi.org/10.1152/ajpregu.00296.2013.

[60] Steiner, A.A., Turek, V.F., Almeida, M.C., Burmeister, J.J., Oliveira, D.L., Roberts, J.L., et al., 2007. Nonthermal activation of transient receptor potential vanilloid-1 channels in abdominal viscera tonically inhibits autonomic cold-defense effectors. Journal of Neuroscience 27(28):7459—7468. https://doi.org/10.1523/JNEUROSCI.1483-07.2007.

[61] Fischer, A.W., Cannon, B., Nedergaard, J., 2019. The answer to the question "What is the best housing temperature to translate mouse experiments to humans?" is: thermoneutrality. Molecular Metabolism 26:1—3. https://doi.org/10.1016/j.molmet.2019.05.006.

[62] Lafontan, M., Langin, D., 2009. Lipolysis and lipid mobilization in human adipose tissue. Progress in Lipid Research 48(5):275—297. https://doi.org/10.1016/j.plipres.2009.05.001.

[63] Collins, S., Kuhn, C.M., Petro, A.E., Swick, A.G., Chrunyk, B.A., Surwit, R.S., 1996. Role of leptin in fat regulation. Nature 380(6576):677. https://doi.org/10.1038/380677a0.

[64] Haynes, W.G., Morgan, D.A., Walsh, S.A., Mark, A.L., Sivitz, W.I., 1997. Receptor-mediated regional sympathetic nerve activation by leptin. Journal of Clinical Investigation 100(2):270—278. https://doi.org/10.1172/JCI119532.

[65] Rahmouni, K., Morgan, D.A., 2007. Hypothalamic arcuate nucleus mediates the sympathetic and arterial pressure responses to leptin. Hypertension 49(3):647—652. https://doi.org/10.1161/01.HYP.0000254827.59792.b2.

[66] Brain, S.D., Williams, T.J., Tippins, J.R., Morris, H.R., MacIntyre, I., 1985. Calcitonin gene-related peptide is a potent vasodilator. Nature 313(5997):54—56. https://doi.org/10.1038/313054a0.

[67] Russell, F.A., King, R., Smillie, S.-J., Kodji, X., Brain, S.D., 2014. Calcitonin gene-related peptide: physiology and pathophysiology. Physiological Reviews 94(4):1099—1142. https://doi.org/10.1152/physrev.00034.2013.

[68] Uddman, R., Edvinsson, L., Ekblad, E., Håkanson, R., Sundler, F., 1986. Calcitonin gene-related peptide (CGRP): perivascular distribution and vaso-dilatory effects. Regulatory Peptides 15(1):1—23. https://doi.org/10.1016/0167-0115(86)90071-6.

[69] Opgaard, O.S., Gulbenkian, S., Bergdahl, A., Barroso, C.P., Andrade, N.C., Polak, J.M., et al., 1995. Innervation of human epicardial coronary veins: immunohistochemistry and vasomotility. Cardiovascular Research 29(4):463—468. https://doi.org/10.1016/S0008-6363(96)88520-8.

[70] Gram, D.X., 2005. Plasma calcitonin gene-related peptide is increased prior to obesity, and sensory nerve desensitization by capsaicin improves oral glucose tolerance in obese Zucker rats. European Journal of Endocrinology 153(6):963—969. https://doi.org/10.1530/eje.1.02046.

[71] Walker, C.S., Li, X., Whiting, L., Glyn-Jones, S., Zhang, S., Hickey, A.J., et al., 2010. Mice lacking the neuropeptide alpha-calcitonin gene-related peptide are protected against diet-induced obesity. Endocrinology 151(9):4257—4269. https://doi.org/10.1210/en.2010-0284.

[72] Zaidi, M., Bevis, P.J., Girgis, S.I., Lynch, C., Stevenson, J.C., MacIntyre, I., 1985. Circulating CGRP comes from the perivascular nerves. European Journal of Pharmacology 117(2):283—284. https://doi.org/10.1016/0014-2999(85)90616-8.

[73] Halloran, J., Lalande, A., Zang, M., Chodavarapu, H., Riera, C.E., 2020. Monoclonal therapy against calcitonin gene-related peptide lowers hyperglycemia and adiposity in type 2 diabetes mouse models. Metabolism Open 8:100060. https://doi.org/10.1016/j.metop.2020.100060.